

1 **Gradual inlet expansion and barrier drowning under**  
2 **most sea level rise scenarios**

3 **Laura Portos-Amill<sup>1,2</sup>, Jaap H. Nienhuis<sup>3</sup>, Huib E. de Swart<sup>1</sup>**

4 <sup>1</sup>Institute for Marine and Atmospheric Research, Department of Physics, Utrecht University, NL

5 <sup>2</sup>Water Engineering and Management, University of Twente, Enschede, NL

6 <sup>3</sup>Department of Physical Geography, Utrecht University, NL

7 **Key Points:**

- 8 • Idealized morphological model simulations show that tidal inlets expand until bar-  
9 rier islands disappear under rapid sea level rise  
10 • Modeled barrier drowning lags sea level rise acceleration by hundreds of years  
11 • Lag in modeled barrier drowning is explained by a decrease in the sand volume  
12 of the barrier

---

Corresponding author: Laura Portos-Amill, [l.portosamill@utwente.nl](mailto:l.portosamill@utwente.nl)

## 13 Abstract

14 The expected increase in rates of sea level rise during the 21st century and beyond  
 15 may cause barrier islands to drown. Barrier drowning occurs due to a sediment imbalance  
 16 induced by sea level rise, causing inlets to open and expand. It is still unclear how  
 17 fast barrier islands can drown. To gain insight into the morphodynamics of barrier systems  
 18 subject to sea level rise, we here present results obtained with a novel barrier island  
 19 exploratory model, BRIE-D, that considers inlet expansion beyond equilibrium size. We  
 20 quantify how much of a barrier island chain is drowned by calculating the fraction  
 21 of its length that is below MSL due to sea level rise. Results show that barrier drowning  
 22 is mostly sensitive to the wave height and the rate of sea level rise. In the model, it  
 23 takes hundreds of years for barrier islands to start drowning in response to high rates  
 24 of sea level rise (more than 5 mm/yr, for a typical coastal environment). This lag in barrier  
 25 response is caused by a gradual decrease in the sand volume of the barrier. Higher  
 26 rates of sea level rise cause earlier and more severe barrier drowning. Modeled barrier  
 27 systems that face higher waves undergo more frequent inlet closures that lower the rate  
 28 of drowning, but they also have a deeper shoreface that increases the rate of drowning.  
 29 In model simulations, the latter process dominates over the former when sea level rise  
 30 rates exceed 5 mm/yr. Model results fairly agree with available field data.

## 31 Plain Language Summary

32 In extreme sea level rise scenarios (like those predicted during the 21st century and  
 33 beyond) barrier islands may drown. Barrier drowning occurs due to a lack of sediment  
 34 induced by sea level rise, which causes submergence of (parts of) the barrier chain. It  
 35 remains difficult to predict when and under which conditions drowning may occur. In  
 36 this study we investigated the dynamics of drowning barrier islands with an exploratory  
 37 numerical model. A key finding from our model is that high rates of sea level rise (higher  
 38 than 5 mm/yr), but also high waves (higher than 1.5 m) result in barrier drowning. How-  
 39 ever, even under model simulations with high rates of sea level rise, it takes a long time  
 40 for the sand in the barrier island to erode. Barrier drowning and disappearance there-  
 41 fore might take hundreds of years. The model results are consistent with available field  
 42 data, but more observations are needed to achieve a full model verification.

## 43 1 Introduction

44 Barrier islands are low-lying coastal land forms that constitute 10 – 15% of the  
 45 world’s coasts (Davis Jr. & FitzGerald, 2010). They lie parallel to the mainland coast,  
 46 thereby they protect it from coastal hazards such as storm surges (Davis Jr. & FitzGer-  
 47 ald, 2010). As most coastal lowlands are densely populated, barrier islands are thus of  
 48 great socio-economic importance.

49 Most barrier islands were created during the Holocene, when rates of relative sea  
 50 level rise (RSLR) decreased from 7–15 mm/yr to  $\sim 2$  mm/yr (Leatherman, 1983; Beets  
 51 & van der Spek, 2000). Different theories about barrier island formation have been pro-  
 52 posed. Barriers may have formed through onshore migration of subtidal bars, or through  
 53 the reworking of sediment after the continental shelf was flooded (Davis Jr. & FitzGer-  
 54 ald, 2010). The latter mechanism is believed to be responsible for the formation of the  
 55 Wadden Islands along the Dutch, German and Danish coast, some 7000 yrs BP (Beets  
 56 & van der Spek, 2000), as well as that of the barrier islands along the US east coast (Fig-  
 57 ure 1).

58 Future projected RSLR is a serious threat to most coastal systems in the world.  
 59 Worst-case scenarios predict a global mean sea level (MSL) increase of roughly 2.7 m by  
 60 the year 2300 compared to the year 2000 (Palmer et al., 2020). Furthermore, the effects

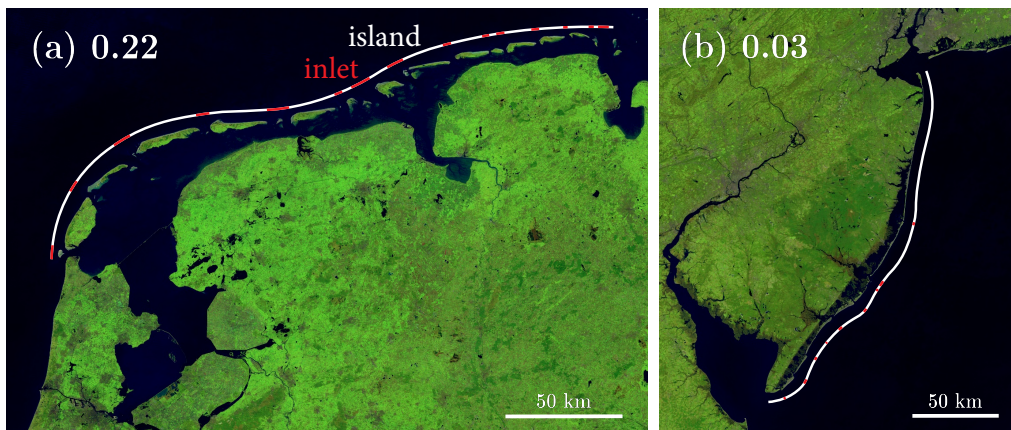


**Figure 1.** Relative sea level rise (RSLR) is expected to increase the fraction of barrier extent below mean sea level (MSL) (Mellett & Plater, 2018). Examples of present-day barrier islands and their respective fraction below MSL (in the alongshore direction): **(a)** 0.22 for the Wadden Islands along the coasts of the Netherlands and Germany, and **(b)** 0.03 for the barrier islands along the US east coast of New Jersey. White curves represent the extent of islands, while red curves represent that of inlets. The given fraction below MSL is computed as the ratio between inlet width and the total barrier chain length (inlets and islands). Extracted from Google Earth (images provided by TerraMetrics).

61 of e.g., vertical land motion should also be considered when studying the response of coastal  
 62 systems to changes in sea level. Given that many barrier islands are located near deltas,  
 63 where land is sinking, they may experience even higher rates of RSLR. Climate change  
 64 may also result in changes in storm return periods, which also affect barrier coasts through  
 65 changes in barrier breaching and sediment transport during overwash events (Reef et al.,  
 66 2020).

67 A possible consequence of this increase in sea level, is that barrier islands will not  
 68 be able to migrate landward fast enough to stay above sea level, resulting in whole-scale  
 69 barrier island drowning (Mellett & Plater, 2018). Drowning, as we define it here in this  
 70 study, is the submergence of (a part of) the barrier island chain due to sediment imbalance  
 71 caused by RSLR. This includes whole-scale barrier drowning, in which the entire  
 72 barrier chain is submerged below MSL, and also partial barrier drowning, in which part  
 73 of the barrier chain is still above MSL and part of it is submerged. Partial barrier drown-  
 74 ing could be a precursor to a whole-scale drowned barrier.

75 Observations of whole-scale drowned barrier systems are scarce. There is an ex-  
 76 ample in the English Channel, where a barrier formed around 9500–8800 yrs BP, when  
 77 MSL was at  $-22$  m relative to that of present day, and it drowned around 8300 yrs BP  
 78 when MSL reached  $-17$  m (Sanders & Kumar, 1975).

79 Observations of partial barrier drowning are more common. An example is the Isles  
 80 Dernières barrier chain (Louisiana, USA), which has been exposed to a rate of RSLR of  
 81 roughly 13 mm/yr since the mid-1800s (Dingler et al., 1993). As a response to this high  
 82 rate of RSLR, new inlets have formed, and existing inlets have widened (FitzGerald et

83 al., 2008). Other modern barrier island chains might also show signs of partial drown-  
84 ing, but this remains poorly quantified.

85 With high rates of RSLR, the part of a barrier island chain that is below MSL (in-  
86 lets, see Figure 1) is expected to increase in the future (Mellett & Plater, 2018). Exist-  
87 ing inlets might have been in equilibrium, due to a balance between sediment export by  
88 tidal currents and sediment import by littoral drift (Escoffier, 1940). But inlet sizes can  
89 increase because RSLR (when ignoring changes in ocean tides) causes an increase in tidal  
90 prism (Stage 2 of the conceptual model of FitzGerald et al., 2008). In addition, RSLR  
91 will create sediment deficits in the barrier chain that will further expand existing inlets  
92 beyond their equilibrium, and also create breaches that will form new inlets (Stage 3 of  
93 the conceptual model of FitzGerald et al., 2008). The threshold rates of RSLR that in-  
94 duce barrier island drowning are mostly unknown, and the subsequent drowning timescales  
95 could be of the order of hundreds of years (Mariotti & Hein, 2022).

96 Here, we study the influence of RSLR on the long-term evolution (hundreds of years)  
97 of barrier island chains. In particular, we focus on the time needed for barrier islands  
98 to respond to changes in rates of RSLR, and on the key mechanisms that drive barrier  
99 island drowning.

100 Process-based models haven been commonly used to investigate barrier drowning.  
101 Stolper et al. (2005) developed the cross-shore GEOMBEST model, which allows for the  
102 study of distinct stratigraphic units characterized by a different erodibility and sediment  
103 composition. Using the GEOMBEST model, Moore et al. (2010) showed the rate of RSLR  
104 to be the main factor determining barrier island drowning. Lorenzo-Trueba and Ash-  
105 ton (2014) designed a cross-shore model to study barrier island drowning and retreat due  
106 to RSLR. They found that a barrier drowns when landward sediment transport on the  
107 shoreface or across the islands is too small to maintain the barrier.

108 Cross-shore models can represent barrier drowning, but their findings are difficult  
109 to compare with observations. This is because they make a binary prediction (a barrier  
110 is either drowned or not) and most modern barrier chains will be somewhere in between.  
111 To study barrier island chains, two horizontal dimensions facilitate easier integration of  
112 models with observations. Such models have been recently developed (Ashton & Lorenzo-  
113 Trueba, 2018; Nienhuis & Lorenzo-Trueba, 2019; Mariotti & Hein, 2022). The model by  
114 Ashton and Lorenzo-Trueba (2018) follows the same parameterized cross-shore dynam-  
115 ics as that of Lorenzo-Trueba and Ashton (2014), and couples them in the alongshore  
116 direction by adding an equation for shoreline evolution that depends on alongshore vari-  
117 ations of the shoreline. The BRIE model of Nienhuis and Lorenzo-Trueba (2019) accounts  
118 for inlet dynamics as well. Moreover, all these processes are included in the model of Mariotti  
119 and Hein (2022), which, in addition, also solves for hydrodynamics. The advantage of  
120 the highly parameterized BRIE model with respect to the more complex model of Mariotti  
121 and Hein (2022) is that it is fast, so it is a suitable tool for performing extensive sensi-  
122 tivity studies. Furthermore, since it explicitly accounts for inlet dynamics, such as open-  
123 ing, closing, or migration, it allows for simulating barrier island states that are in between  
124 fully emerged and fully drowned. However, BRIE only considers inlets that are in mor-  
125 phodynamic equilibrium (i.e., following Escoffier, 1940) and does not consider the dy-  
126 namic effects of RSLR on inlets.

127 Motivated by the existing modeling restrictions, we modify and expand the BRIE  
128 model into the BRIE-D model to allow for RSLR-driven transformations of tidal inlets  
129 on barrier island chains. Note that both BRIE and BRIE-D are ‘exploratory’ models (Murray,  
130 2003), aiming at understanding a poorly understood process (here, barrier drowning) rather  
131 than representing a specific barrier island.

132 Our study objectives are to (1) understand the effects of RSLR on the barrier is-  
133 land sediment balance, inlet expansion and the related barrier drowning, (2) examine

134 the temporal evolution of inlet expansion in a drowning barrier, and (3) explore the de-  
 135 pendence of barrier island drowning on model parameters (e.g., wave height, rate of RSLR,  
 136 storm return period, tidal amplitude).

137 The next section includes a description on how barrier drowning is quantified and  
 138 modeled, together with the design of simulations and analysis of model output. Section 3  
 139 contains the results, followed by a discussion in Section 4. The final section contains the  
 140 conclusions.

## 141 2 Methods

### 142 2.1 Metrics for Studying Barrier Island Drowning

143 In this study, we use a measure for RSLR-driven barrier island drowning that is  
 144 derived as follows. Consider a barrier island chain, with an alongshore extent  $L_b$ , sep-  
 145 arated by  $N$  different inlets, each having a width  $W_{inlet,i}$ , where  $i = 1, 2, \dots, N$ . In the  
 146 course of time, the number of inlets  $N$  may change as a result of islands becoming drowned,  
 147 barrier storm breaching, inlet closure, and inlets merging. The width of each inlet may  
 148 also change, and expand to become very wide with tips that are morphologically discon-  
 149 nected. We define the fraction of barrier extent that is drowned  $\Delta F$  as

$$150 \quad \Delta F = F - F_{eq}, \quad F = \frac{\sum_{i=1}^N W_{inlet,i}}{L_b}, \quad F_{eq} = \frac{\sum_{i=1}^N W_{inlet,eq,i}}{L_b}. \quad (1)$$

151 In this expression,  $F$  is the fraction of barrier extent below MSL (i.e., the part of  $L_b$  that  
 152 consists of inlets, see e.g. Figure 1). However,  $F$  itself is not characterizing barrier drown-  
 153 ing, as inlets do exist under non-drowning conditions. In the latter case, the inlets are  
 154 said to be in equilibrium. The equilibrium widths of the inlets are denoted by  $W_{inlet,eq,i}$ ,  
 155 from which it follows the fraction  $F_{eq}$  of the barrier below MSL. As shown by Equation 1,  
 156 it is the difference between  $F$  and  $F_{eq}$ , i.e., the fraction  $\Delta F$  of the barrier length below  
 157 MSL due to tide-wave imbalance, that quantifies how much of a barrier is drowned.

158 Note that a single inlet can be comprised of a part that is due to equilibrium, and  
 159 another part due to drowning (see Figure 2 for a graphical example). The fraction of bar-  
 160 rier extent that is drowned varies between 0 and 1. If  $\Delta F = 0$ , the barrier, on aver-  
 161 age, is in morphological equilibrium. Barrier drowning starts taking place when  $\Delta F >$   
 162 0, which may precede a whole-scale drowned barrier.

163 Variations in  $F$  are caused by different mechanisms. Human modifications to bar-  
 164 riers (constructing jetties, maintaining inlets, nourishments, etc.) cause deviations in the  
 165 fraction of barrier extent below MSL. Short-term natural dynamics (storm breaching,  
 166 inlet migration, etc.) also cause  $F$  to deviate away from its equilibrium. Here, we focus  
 167 on RSLR, which affects  $\Delta F$  but also  $F_{eq}$  through modifications of the tidal prism (FitzGerald  
 168 et al., 2008). Section 2.3 describes how  $\Delta F$  is computed from (BRIE-D model) data.

### 169 2.2 Model Description

170 We use the morphological BRIE-D model to study barrier drowning (measured with  
 171  $\Delta F$ ). We also use the BRIE model to simulate the evolution of a barrier chain that is  
 172 always in equilibrium, thus not drowning. BRIE-D is an extension of the BRIE model  
 173 (Nienhuis & Lorenzo-Trueba, 2019). The main differences between the two models are  
 174 the following. In the original BRIE model, inlets are prescribed to have an equilibrium  
 175 width ( $F = F_{eq}$ , such that  $\Delta F = 0$ ). We modified BRIE into BRIE-D, in which a dy-  
 176 namic evolution of inlets is allowed that depends on the sediment mass balance. In this  
 177 section, we describe inlet formation and evolution. Further details on the other model  
 178 routines (e.g., cross-shore dynamics, shoreline evolution and numerical aspects) are given  
 179 in the Supplementary Information (SI1). More details about the BRIE model are given  
 180 in Nienhuis and Lorenzo-Trueba (2019). In this paper, we compare BRIE-D to BRIE to

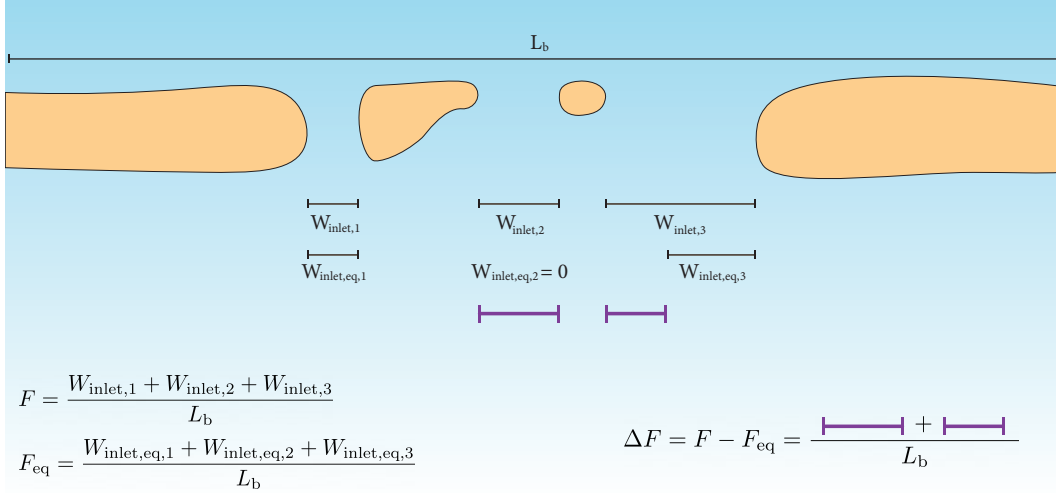


**Figure 2.** Graphical example of how the variables  $F$ ,  $F_{eq}$  and  $\Delta F$ , which measure various aspects of drowning in our model, are defined. A chain (with total alongshore length  $L_b$ ) of four barrier islands (yellow) and three inlets (widths  $W_{inlet,1,2,3}$ ) is shown. In this case, Inlet 1 is in equilibrium ( $W_{inlet,1} = W_{inlet,eq,1}$ ), Inlet 2 is fully drowned ( $W_{inlet,eq,2} = 0$ , i.e., according to equilibrium inlet theory it should be closed, but due to drowning of a portion of the barrier it is open), and the width of Inlet 3 consists of an equilibrium component and a drowned component. Purple segments represent the (parts of) inlet widths contributing to  $\Delta F$ .

181 investigate the effect of inlet dynamics on barrier drowning, and we use BRIE-D to then  
 182 investigate barrier island drowning timescales. All results are from the (newer) BRIE-D,  
 183 unless specified.

### 184 **2.2.1 Inlet Opening**

185 The BRIE-D model considers a barrier-inlet system with a given alongshore extent  
 186  $L_b$ . Initially, there are no inlets, but they can appear in two different ways. Inlets may  
 187 open either due to barrier breaching caused by a storm or due to barrier drowning. Breach-  
 188 ing is imposed every  $T_{storm}$  years where the barrier volume is at a minimum, and at a  
 189 location at least 5 km from existing inlets (Roos et al., 2013). The time  $T_{storm}$  is to be  
 190 interpreted as a storm return period. The initial width of a breached inlet is set at 1 km.

191 Alternatively, inlets appear when a portion of the barrier drowns (either because  
 192 the width or the height of the barrier becomes negative), which is not restricted to its  
 193 proximity to other inlets. The initial width of a drowned inlet is set equal to the width  
 194 of the portion of the barrier that drowned.

### 195 **2.2.2 Inlet Evolution**

196 Once inlets exist, the BRIE-D model calculates their widths and equilibrium widths  
 197 (needed to calculate  $F$ ,  $F_{eq}$  and  $\Delta F$ ) as follows. First, inlet width  $W_{inlet}$  is related to  
 198 cross-sectional area  $A_{inlet}$  by assuming a prismatic cross-section and a depth-to-width  
 199 ratio (or aspect ratio)  $\gamma_{aspect}$ . The inlet aspect ratio is assumed to be constant only for  
 200 small inlets. Based on observations (Hume & Herdendorf, 1992), the maximum inlet depth  
 201 is set at 15 m, above which an increase in inlet cross-sectional area causes an increase  
 202 in only the inlet width. Denoting the depth by  $D_{inlet}$ , it follows that  $A_{inlet} = W_{inlet}D_{inlet} =$

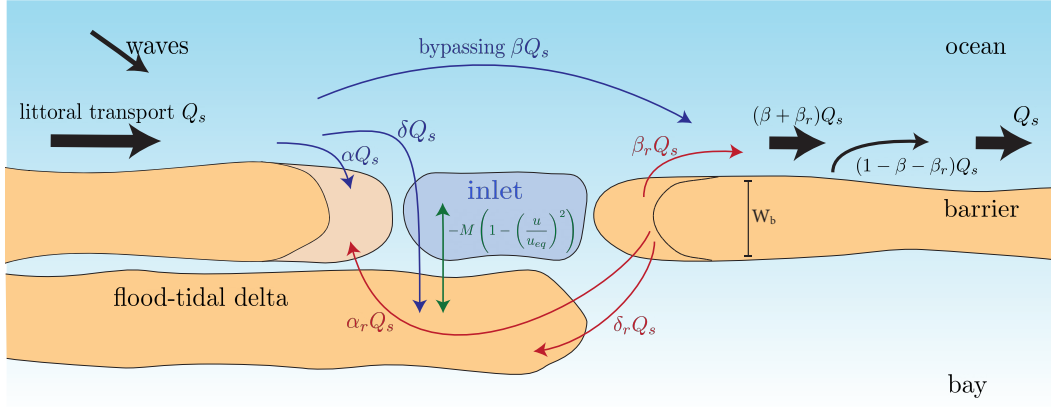


**Figure 3.** Sketch of the different elements of an inlet system and the mass exchanges with updrift and downdrift tips of the barrier, as well as with the flood-tidal delta. The parameters  $\alpha$ ,  $\beta$ ,  $\delta$ ,  $\alpha_r$ ,  $\beta_r$  and  $\delta_r$  denote fractions of the littoral transport  $Q_s$ . Note that the flood-tidal delta extends through the updrift barrier because it has been building up as the inlet was migrating. Modified from Nienhuis and Lorenzo-Trueba (2019) and Nienhuis and Ashton (2016). A detailed description of the moving boundaries and the sediment exchange within the inlet is given in SI1.

203  $\gamma_{aspect} W_{inlet}^2$ , so

204 
$$W_{inlet} = (A_{inlet}/\gamma_{aspect})^{1/2}, \quad W_{inlet,eq} = (A_{inlet,eq}/\gamma_{aspect})^{1/2}. \quad (2)$$

205 Now,  $A_{inlet,eq}$  is calculated using the Escoffier (1940) relation, i.e. from a balance be-  
 206 tween sediment import by waves and sediment export by tides (which depends on  $A_{inlet}$   
 207 and given tidal conditions). Details are given in SI1, Equations 61–64.

208 The evolution of the actual cross-sectional area  $A_{inlet}$  is governed by four drivers,

209 
$$\frac{dA_{inlet}}{dt} = G_{sd} + G_{Esc} + G_m + G_d. \quad (3)$$

210 The first driver is  $G_{sd}$ , which represents the change in cross-sectional area resulting from  
 211 the relative accretion and erosion of each inlet flank. As is shown in Figure 3, a fraction  
 212  $\alpha + \alpha_r$  (depending on wave and tidal condition) of the alongshore wave-driven sediment  
 213 transport  $Q_s$  is deposited on the tip of the updrift island, causing the updrift inlet flank  
 214 to move at a rate  $dL_{up}/dt$ . Likewise, a certain fraction  $\beta_r + \delta_r + \alpha_r$  of sediment is eroded  
 215 from the downdrift inlet flank, causing it to move at a rate  $dL_{down}/dt$ . In the BRIE model,  
 216 these deposition and erosion processes only result in migration of the inlet, and the value  
 217 of  $\delta_r$  is chosen such that inlet width is kept constant. In the BRIE-D model this con-  
 218 straint is released, resulting in variations in the cross-sectional area of the inlet, leading  
 219 to

220 
$$G_{sd} = D_{inlet} \left( \frac{dL_{down}}{dt} - \frac{dL_{up}}{dt} \right). \quad (4)$$

221 In the BRIE model this sediment distribution was such that the cross-sectional area of the  
 222 inlet was maintained constant. In the BRIE-D model we allow for both tips of the  
 223 barrier to be disconnected, and grow or shrink the inlet. A description of the variations  
 224 in updrift and downdrift sediment volumes is given in SI1, Equations 32–40.

225 We further allow for variations in the cross-sectional area of the inlet depending  
 226 on the sediment exchange with the flood-tidal delta. This sediment exchange depends  
 227 on a prescribed transport from the flood-tidal delta to the inlet and the export of sed-  
 228 iment from the inlet to the flood-tidal delta due to tidal currents. For this, a simple model

229 for an inlet-bay system is employed, as was used by Escoffier (1940) to explain the sta-  
 230 bility of tidal inlets. The changes on the cross-sectional area of the inlet governed by these  
 231 dynamics are described by

$$232 \quad G_{Esc} = -\frac{M}{W_b} \left( 1 - \left( \frac{U}{U_e} \right)^2 \right). \quad (5)$$

233 In this equation,  $W_b$  is the width of the barrier and  $U$  is the amplitude of the tidal cur-  
 234 rent in the inlet (which depends on the imposed tidal amplitude at sea, the cross-sectional  
 235 area of the inlet, the barrier width, and the wetted surface of the back-barrier lagoon).  
 236 Furthermore,  $U_e$  is the amplitude of the tidal current at equilibrium (set at 1 m/s for  
 237 all simulations), and  $M$  is the volume of sediment per time unit that the inlet receives  
 238 from the flood tidal delta. With this representation of tidal dynamics we allow for the  
 239 inlet to evolve toward an equilibrium configuration, using a parametrization of the net  
 240 sediment transport due to tides that was earlier used by van de Kreeke (2004).

241 A third way inlets can increase their cross-sectional area is by merging with other  
 242 inlets. The increase in the cross-sectional area of the inlet due to merging with other in-  
 243 lets  $G_m$  is such that the total cross-sectional area is conserved. As a result, if inlets  $j$   
 244 and  $k$  merge, with  $j < k$ , the cross-sectional area of inlet  $j$  is then  $A_{inlet,j} + A_{inlet,k}$ ,  
 245 and inlet  $k$  is no longer present at the next time step.

246 Lastly, the increase in the cross-sectional area of the inlet due to barrier drown-  
 247 ing depends on the length  $W_d$  of the portion of the barrier that drowned (due to either  
 248 a negative barrier width or a negative barrier height),

$$249 \quad G_d = \frac{dW_d}{dt} \gamma_{aspect} W_d. \quad (6)$$

250 In the case of barrier drowning, it may be that, according to the inlet aspect ratio for-  
 251 mulation, the inlet is deeper than the initial depth of the drowned portion of the bar-  
 252 rier. In order to ensure sediment conservation, the sediment missing in the inlet is added  
 253 to the flood-tidal delta.

### 254 **2.3 Analysis of Model Output**

255 We study the barrier response to RSLR through  $F$ ,  $F_{eq}$  and  $\Delta F$ . Values for  $F$ ,  $F_{eq}$   
 256 and  $\Delta F$  are computed from  $W_{inlet}$  and  $W_{inlet,eq}$ , which are output of the models. Note  
 257 that the value of  $F_{eq}$  obtained with the BRIE-D model, which allows for a gradual evo-  
 258 lution of inlets, will not be necessarily identical to the value of  $F$  obtained with the BRIE  
 259 model, which imposes inlets to be in equilibrium. This is because the time evolution of  
 260 both models is governed by different dynamics (Equation 3 in the BRIE-D model, al-  
 261 lowing for a gradual evolution, versus the immediate equilibrium imposed in the BRIE  
 262 model). Indeed, the different processes implemented in the BRIE-D model interact with  
 263 each other, resulting in non-linear dynamics. Thus, the number and distribution of in-  
 264 lets will be different in both models. This difference in number and distribution of in-  
 265 lets may lead to, for example two inlets being closer in BRIE-D than in BRIE, produc-  
 266 ing different equilibrium inlet widths, and hence different values of  $F_{eq}$  in BRIE-D from  
 267 the  $F$  in BRIE.

268 We study the timescales involved in barrier drowning by investigating the timeseries  
 269 of  $\Delta F$  under increasing rates of RSLR. Two timescales are defined: first, the time it takes  
 270 until  $\Delta F$  exceeds 0.1, and, second, the time it takes until  $\Delta F$  exceeds 0.3. Here, the time  
 271 at which  $\Delta F = 0.1$  represents the moment at which a noticeable amount of drowning  
 272 has occurred. The time at which  $\Delta F = 0.3$  or, in other words, the situation where RSLR  
 273 has submerged 30% of the barrier alongshore extent, represents the time at which an ag-  
 274 gravated drowning has occurred and the barrier is even more prone to eventually fully  
 275 drown.

276 We also study the time evolution of other morphological metrics of drowning bar-  
 277 riers, namely the number of inlets and the barrier width. The latter is represented by  
 278 its alongshore mean through time, and it is computed as the distance between the sea-  
 279 ward shoreline and the back-barrier shoreline. We compute the barrier width only along  
 280 the parts corresponding to subaerial barrier, i.e., where  $W_b > 0$ .

## 281 2.4 Design of Simulations

282 Our first aim is to understand the effects of RSLR on the barrier island sediment  
 283 balance, inlet expansion and the related barrier drowning. We compare the evolution of  
 284 a barrier system in which inlets are imposed to be in equilibrium to that of a barrier in  
 285 which inlets dynamically evolve, depending on the sediment balance. We used the BRIE  
 286 and BRIE-D models for each of these situations, respectively, both with the same input  
 287 parameters. For the two situations, we further compare the evolution of the barrier for  
 288 two rates of RSLR ( $\dot{\xi} = 4, 17$  mm/yr) to represent a situation close to equilibrium, and  
 289 a situation with drowning.

290 To achieve the second aim, i.e., to examine the temporal evolution of inlet expan-  
 291 sion in a drowning barrier, we performed simulations with the BRIE-D model for  $\dot{\xi} =$   
 292 17 mm/yr. For the sake of comparison, we also include the situation that  $\dot{\xi} = 4$  mm/yr  
 293 (no drowning).

294 To achieve the third aim (quantify dependence of barrier island drowning on model  
 295 parameters), we performed simulations with a broad range of significant wave heights,  
 296 rate of RSLR, storm return period, wave period, wave asymmetry, inlet aspect ratio, max-  
 297 imum overwash transport, and the suspended sediment transport efficiency factor, which  
 298 controls the shoreface transport. These are also performed with the BRIE-D model, in  
 299 order to allow for a dynamic evolution of the inlets and study their effects on barrier drown-  
 300 ing.

301 All simulations have a run time of 2500 yrs, taking  $\dot{\xi} = 2$  mm/yr during the first  
 302 2000 yrs, which serves as model spin-up period. After model spin-up, when the system  
 303 reaches a statistically stationary state in terms of inlet number and inlet migration rates,  
 304 we change  $\dot{\xi}$  in order to study the system response for another 500 yrs. All other param-  
 305 eters have values that are representative for a typical mid-latitude barrier island chain  
 306 and are kept constant during the entire 2500 yrs (see Appendix A for a full overview of  
 307 the model parameters and their default values). The new  $\dot{\xi}$  is not changed during the  
 308 last 500 yrs of model evolution. Note that we do not aim to simulate any barrier sys-  
 309 tem specifically, but to get a broad picture of barrier response to RSLR. Table 1 presents  
 310 an overview of the simulations performed.

311 Since we deal with a stochastic system, where randomness originates from the wave  
 312 angle and from the initial conditions (see SI1), we performed five model realizations for  
 313 each parameter setting. We present the model results as the mean of the five realizations  
 314 for each parameter setting. Errors are quantified using the standard error of the mean.  
 315 Experiments performed with an ensemble size of 100 showed no significant differences  
 316 in model outcome when compared to results computed with only five simulations.

## 317 3 Results

### 318 3.1 Effects of Dynamic Inlets on RSLR-induced Barrier Drowning

319 An example BRIE-D model simulation allowing for dynamic inlets under a rate of  
 320 RSLR  $\dot{\xi} = 17$  mm/yr shows a gradual expansion of inlets during 500 yrs of barrier evo-  
 321 lution (Figure 4). The barrier appears to drown gradually: initially (after the model spin-  
 322 up period), the barrier is in a statistical equilibrium state. After 200 yrs drowning starts  
 323 ( $\Delta F = 0.2$ ), and after 400 yrs more than half of the alongshore extent of the barrier

**Table 1.** Overview of simulations performed, imposing different values for the rate of RSLR ( $\dot{\xi}$ ) and significant wave height ( $H_s$ ).

Aim	Model used	Parameter range <sup>a</sup>	Figure
Effects of RSLR on inlet sediment balance	BRIE, BRIE-D <sup>b</sup>	$\dot{\xi} = 4, 17$ mm/yr	4, 5
Temporal evolution of barrier drowning	BRIE-D	$\dot{\xi} = 4, 17$ mm/yr	6
Dependence on model parameters	BRIE-D	$\dot{\xi}$ varying between 2 and 20 mm/yr, $H_s$ varying between 0.75 and 3 m <sup>c</sup>	7, 8, 9

<sup>a</sup> If not specified parameters take their default values (see Appendix A).

<sup>b</sup> Same input parameters for both models.

<sup>c</sup> Mulhern et al. (2017)

324 is below MSL ( $\Delta F = 0.6$ ). The transition from a state in which inlets are in morpho-  
 325 dynamic equilibrium towards a state of drowning is evident after 200 yrs, as some in-  
 326 lets become much wider than in the equilibrium situation ( $\sim 7$  km). From there on, in-  
 327 lets merge and widen to the order of tens of km by the year 400.

328 In order to understand the potential effects of RSLR on inlet expansion and the  
 329 related barrier drowning, we performed simulations allowing for a gradual evolution of  
 330 inlets depending on the barrier sediment balance. We compare their output to that of  
 331 simulations in which inlets are imposed to be in equilibrium. To study the effects of RSLR,  
 332 we use low and high rates of RSLR ( $\dot{\xi} = 4$  mm/yr and  $\dot{\xi} = 17$  mm/yr, respectively).  
 333 Recall that for all simulations a spin-up period of 2000 yrs with  $\dot{\xi} = 2$  mm/yr is used.

334 For low  $\dot{\xi}$ , there are differences in barrier evolution between the situation in which  
 335 inlets are imposed to be in equilibrium and the situation in which they are allowed to  
 336 gradually evolve (Figure 5a,b), albeit that no drowning occurs in this case. Inlets tend  
 337 to close more easily when they can gradually evolve in time (Figure 5a). This is because  
 338 they are allowed to be closer to the “unstable equilibrium” (Equation 5, Escoffier, 1940),  
 339 when inlet narrowing starts to decrease inlet flow velocities below the equilibrium ve-  
 340 locity. In addition, independent updrift and downdrift flank migration rates (Equation 4)  
 341 will also cause a greater instability in inlet size, which could lead to more frequent clo-  
 342 sure (as well as inlets larger than the stable equilibrium). Nevertheless, on longer timescales,  
 343 low RSLR rates also lead to relatively steady inlet widths over time, similar to model  
 344 simulations with the equilibrium imposed (Figure 5b). Furthermore, inlet migration rates  
 345 are generally similar in both situations ( $\sim 1-2$  m/yr), with the exception of short pe-  
 346 riods in which dynamic inlets migrate at rates of order 200 m/yr, due to local narrow-  
 347 ing of the barrier. These low rates of RSLR do not present signs of an adaptation pe-  
 348 riod to the new value of  $\dot{\xi}$  imposed at  $t = 0$ .

349 Simulations under high rates of RSLR ( $\dot{\xi} = 17$  mm/yr) reveal that when inlets  
 350 are imposed to be in equilibrium, the response of the system strongly differs from that  
 351 in which inlets can gradually evolve (Figure 5c,d). In general, imposing equilibrium yields  
 352 an irregular evolution of inlet widths, with abrupt changes taking place for example at  
 353 the years 450 and 465, or with inlet closing briefly after opening at years 350–400. This  
 354 behavior is due to barrier drowning being disconnected from (other) inlet dynamics. In  
 355 contrast, by allowing for feedbacks between tide-induced inlets and drowning-induced  
 356 inlets, we see more gradual inlet evolution. The resulting barrier behavior is smoother,  
 357 but also a faster increase in  $\Delta F$  is seen. Another difference between the non-equilibrium  
 358 (BRIE-D, Figure 5c) and equilibrium (BRIE, Figure 5d) inlet model for  $\dot{\xi} = 17$  mm/yr  
 359 is the resulting inlet migration rate. The non-equilibrium model yields higher migration

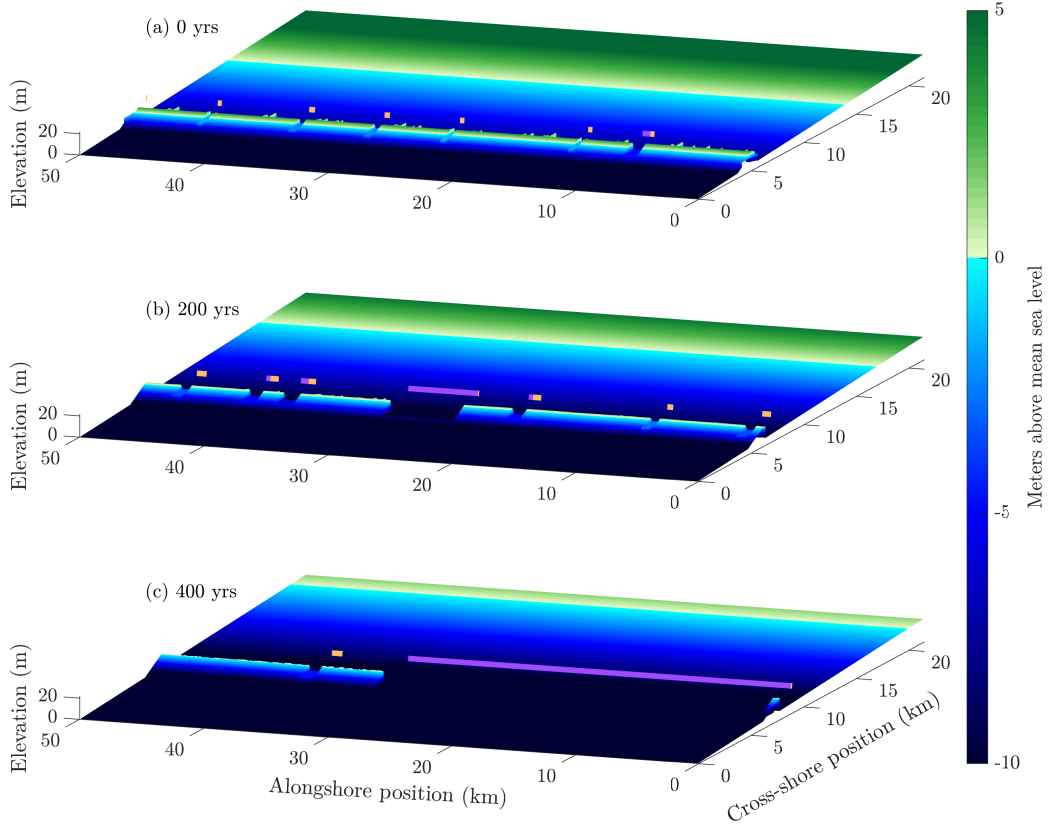


**Figure 4.** Modeled barrier island evolution (accounting for dynamic inlet evolution) at (a) 0, (b) 200 and (c) 400 years after the model spin-up period. Simulation is for a rate of RSLR  $\dot{\xi} = 17$  mm/yr and for a domain with an along-shore extent of 50 km. Orange lines represent the equilibrium width for each inlet ( $W_{inlet,eq}$ ) and purple lines the difference between the actual inlet width and that at equilibrium. All parameters except  $\dot{\xi}$  have their default values (see Table A1); in particular the offshore significant wave height is  $H_s = 1.5$  m and the tidal amplitude is  $a_0 = 0.8$  m.

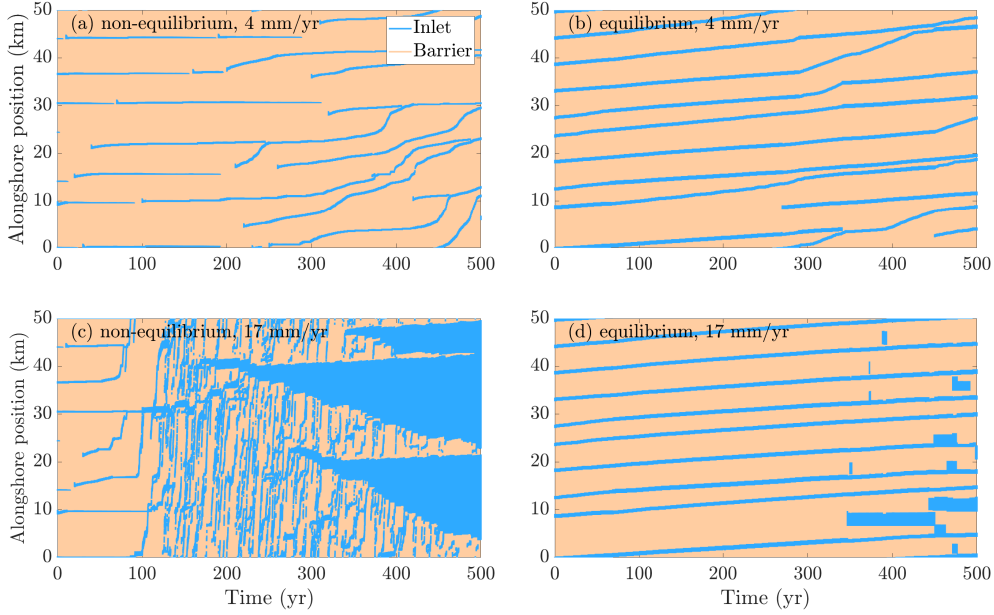


**Figure 5.** Comparison between the output of a model that allows for a gradual evolution of the cross-sectional area of the inlets (BRIE-D), and that of a model imposing inlets to be in equilibrium (BRIE): Temporal evolution of barrier systems during 500 yrs in a 50 km long domain for a  $\dot{\xi}$  of **(a,b)** 4 mm/yr (barrier drowning is not occurring) and **(c,d)** 17 mm/yr (there is barrier drowning causing widening the inlets). Simulations **(a,c)** allow for a gradual evolution of the inlets, whilst in simulations **(b,d)** inlets attain equilibrium instantaneously. All parameters except  $\dot{\xi}$  have their default values (see Table A1); in particular the offshore significant wave height is  $H_s = 1.5$  m and the tidal amplitude is  $a_0 = 0.8$  m.

360 rates ( $\sim 5$  km/yr) compared to the equilibrium model ( $\sim 10$  m/yr) for narrow inlets  
 361 ( $< 2$  km). These high migration rates appear when the barrier is very narrow ( $< 100$  m).  
 362 The difference between the two models is caused by the updrift and downdrift barrier  
 363 tips evolving independently ( $G_{sd}$ , Equation 4), imposed to allow for inlet widening be-  
 364 yond its equilibrium state. This disconnection causes differences in sediment deposition  
 365 in the inlet, which alters inlet migration. Note the time lag in barrier response in the BRIE-D  
 366 model after the rate of RSLR has increased from 2 to 17 mm/yr at  $t = 0$ . It takes 100–  
 367 150 yrs for the barrier to adapt to the new conditions.

### 368 **3.2 Evolution of a Drowning Barrier**

369 Allowing for non-equilibrium inlets in a drowning barrier affects the temporal evolu-  
 370 tion of  $F$ ,  $\Delta F$ ,  $F_{eq}$ , barrier width  $W_b$  and the number of inlets (Figure 6). In the case  
 371 of dynamic inlets and a high rate of RSLR ( $\dot{\xi} = 17$  mm/yr), Figure 6b shows that  $F$   
 372 gradually increases from the year 100 up to  $\sim 0.8$  after 500 yrs. When inlet equilibrium  
 373 is imposed,  $F$  also increases, due to an increase in tidal prism, reaching values up to 0.3.  
 374 This increase in  $F$  corresponds to the sudden inlet creation and inlet widening taking  
 375 place from the year 350 onward (see Figure 5e). Gradually evolving inlets result in a grad-  
 376 ually increasing  $F$  from the year  $\sim 100$ . The situation with a low rate of RSLR ( $\dot{\xi} =$   
 377 4 mm/yr) shows a constant  $F$  for both situations.

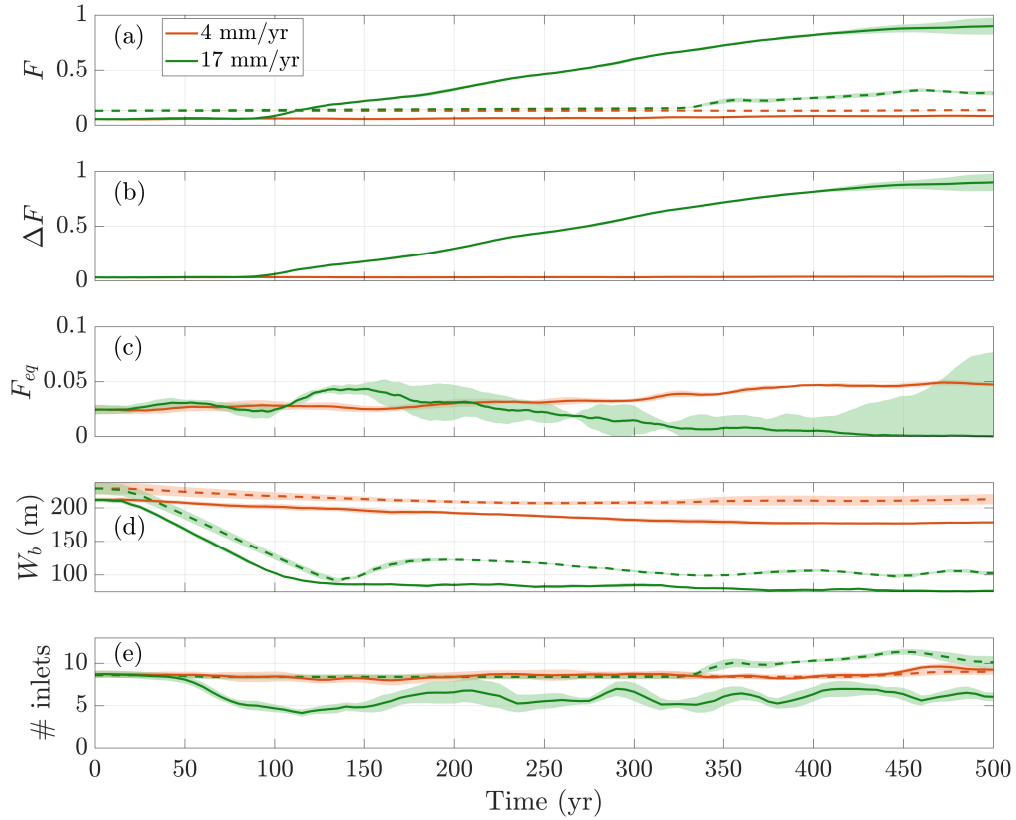


**Figure 6.** (a) Time series of  $F$  for  $\dot{\xi} = 4$  mm/yr and  $\dot{\xi} = 17$  mm/yr, comparing barrier drowning under non-equilibrium inlet dynamics (solid) and equilibrium inlet dynamics (dashed). (b) As (a), but for  $\Delta F$  (only for non-equilibrium inlet dynamics because  $\Delta F = 0$  for inlets in equilibrium). (c) As (b), but for  $F_{eq}$ . (d) As (a), but for mean barrier width  $W_b$ . (e) As (a), but for the number of inlets. Curves represent the mean over five simulations. Shaded areas represent the standard error of the mean. Note the different scales of the vertical axes.

When allowing for dynamic inlets,  $\Delta F$  is much larger than  $F_{eq}$  for  $\dot{\xi} = 17$  mm/yr (see Figure 6b,c), meaning that drowning is the main process through which inlets are created and maintained open. The fraction  $\Delta F$  starts to deviate from zero after 100 yrs of evolution when  $\dot{\xi} = 17$  mm/yr, and achieves a value of 0.8 after 400 yrs more. In contrast, the simulation during which  $\dot{\xi} = 4$  mm/yr is always close to equilibrium, i.e.,  $\Delta F$  is always close to zero with a maximum deviation of 0.001. In this situation of low rate of RSLR, the barrier moves landward without losing mass or subaerial surface area. Accordingly,  $\Delta F$  remains constant. This means that landward migration of the barrier sufficiently offsets lagoon widening to prevent severe changes in the tidal prism and thus drowning from increases in tidal prism does not occur. This is consistent with observations from Deaton et al. (2017).

The fraction  $F_{eq}$  decreases until reaching a value of 0 after 500 years of evolution for  $\dot{\xi} = 17$  mm/yr. This is because  $F_{eq}$  is a metric arising from each individual inlet (not the barrier chain as a whole), thus it decreases when the barrier starts to drown and inlets starts to merge. With  $\dot{\xi} = 4$  mm/yr,  $F_{eq}$  slightly increases from 0.025 to 0.05 because of a small increase in tidal prism caused by lagoon widening.

Barrier width rapidly decreases in the simulations with  $\dot{\xi} = 17$  mm/yr during the first  $\sim 100 - 150$  yrs of evolution after spin-up (see Figure 6d). This means that the sediment reservoir of the barrier (its sediment volume) starts decreasing briefly (less than 30 yrs) after the barrier is exposed to a new rate of RSLR. This period is a transition period, in which the barrier is adjusting to the new  $\dot{\xi}$ . There is also a minor decrease in barrier width for the case  $\dot{\xi} = 4$  mm/yr, regardless of the inlets being always close to equilibrium. The barrier width eventually reaches an equilibrium value that depends on the  $\dot{\xi}$  imposed. That value is about 30 m larger when imposing inlet equilibrium instead of allowing for a gradual inlet evolution for the two values of  $\dot{\xi}$  shown. This difference is due to the added inlet dynamics in the latter situation. Adding sediment exchange between the inlet and the flood-tidal delta decreases sediment availability along the barrier islands, thereby reducing the barrier width.

Both configurations, i.e., equilibrium and non-equilibrium inlet dynamics, produce roughly the same number of inlets for  $\dot{\xi} = 4$  mm/yr (Figure 6e), because the inlets are close to equilibrium (i.e.,  $\Delta F \sim 0$ ). In equilibrium, the number of inlets is controlled solely by the available tidal prism and the alongshore distance at which inlets remain stable (Roos et al., 2013). Thus, the number of inlets remains constant at  $\sim 8-9$ . For faster RSLR ( $\dot{\xi} = 17$  mm/yr), equilibrium and non-equilibrium inlets start to behave differently. The number of inlets fluctuates between 8 and 9 when imposing equilibrium, showing no big differences with the situation with lower  $\dot{\xi}$  until the year 350. After 350 yrs, it increases up to  $\sim 11-12$ . In contrast, when letting inlets gradually evolve in time, the number of inlets decreases to  $\sim 5-6$  and fluctuates around these numbers from the year  $\sim 200$  onward. This is because inlets are wider when they are not restricted to be in equilibrium, thus there is less subaerial portion of the barrier where inlets may form and survive without merging with other existing inlets.

### 3.3 Wave Height and RSLR Effects on Barrier Drowning

We performed a sensitivity analysis for the main parameters that control the system: tidal amplitude, significant wave height, wave period, rate of RSLR, wave asymmetry, inlet aspect ratio, storm return period, maximum overwash transport and the suspended sediment transport efficiency factor, which controls the shoreface transport. The significant wave height  $H_s$  and the rate of RSLR  $\dot{\xi}$  turned out to be the parameters with the strongest impact on barrier drowning. The full sensitivity analysis is presented in Appendix B.

The fraction of barrier extent below MSL,  $F$ , changes due to the variations in  $F_{eq}$ , and in  $\Delta F$ . Here,  $F_{eq}$  shows a dependence on significant wave height  $H_s$  and rate of RSLR

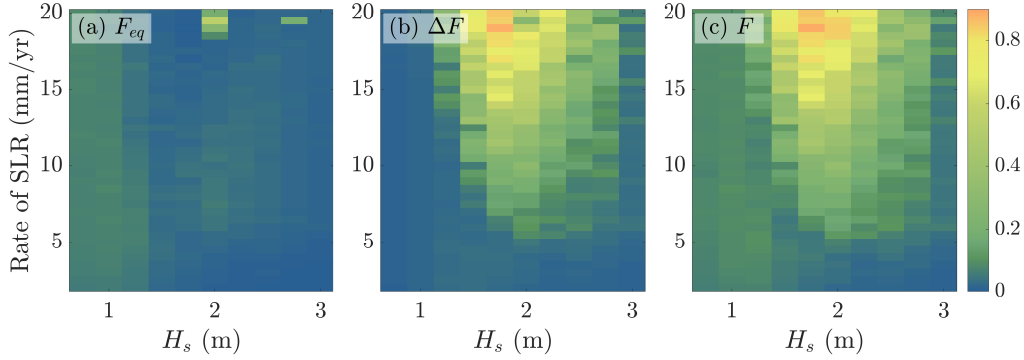


**Figure 7.** For different values of significant wave height  $H_s$  and rate of RSLR  $\dot{\xi}$ : (a) the fraction of barrier extent below MSL, assuming an equilibrium situation for the inlets ( $F_{eq}$ ), (b) the fraction of barrier extent below MSL due to tide-wave imbalance in the inlet ( $\Delta F$ ), (c) the fraction of barrier extent below MSL ( $F_{eq} + \Delta F = F$ ) at the year 300.

429  $\dot{\xi}$  (see Figure 7a). This dependence is mainly caused by variations in tidal prism and sedi-  
 430 ment imported into the inlets by the littoral drift. For example, higher waves cause a  
 431 decrease in  $F_{eq}$ , because they tend to close existing inlets. Nevertheless, variations in  $F_{eq}$   
 432 are low compared to the effects of drowning (see Figure 7b). There are two mechanisms  
 433 that explain why  $\Delta F$  shows more variations than  $F_{eq}$ . Firstly, RSLR results in thinner  
 434 barriers, decreasing barrier volume, and thereby higher  $G_{sd}$ . Secondly, waves affect shoreface  
 435 sediment transports, increasing the potential onshore sediment transport, but also the  
 436 shoreface depth (see SI1), leading to higher  $\Delta F$  for intermediate wave height. The behav-  
 437 ior of  $F$  is only dominated by that  $F_{eq}$  for low rates of RSLR ( $\dot{\xi} < 5$  mm/yr), where  
 438 the effect of RSLR is lower (see Figure 7c).

439 Overall, the results of Figure 8 reveal that an increase in  $\dot{\xi}$  causes more drowning,  
 440 as  $\Delta F$  eventually takes larger values (see Figure 8a1, b1, c1).  $\Delta F$ , deviates from zero  
 441 for rates of RSLR larger than a certain threshold ( $\dot{\xi} \sim 6$  mm/yr). For  $\dot{\xi}$  lower than 6 mm/yr,  
 442 maximum differences in  $\Delta F$  are 0.04 by the year 500. A similar general dependency of  
 443 the barrier width  $W_b$  on the rate of RSLR is seen (Figure 8a2, b2, c2), which attains lower  
 444 values at latter times and at higher  $\dot{\xi}$ . Yet,  $W_b$  responds earlier to changes in  $\dot{\xi}$ , present-  
 445 ing more variability with respect to the initial value than  $\Delta F$  after  $t = 100$  yrs. Note  
 446 that these values depend on other parameters as well (e.g., tidal amplitude, maximum  
 447 overwash transport).

448 The number of inlets does not show such a clear dependence on  $H_s$  and  $\dot{\xi}$  as  $\Delta F$   
 449 or  $W_b$  (see Figure 8a3, b3, c3). Specifically, there are some cases with RSLR-driven drown-  
 450 ing with a low number of inlets with (some of) them being very wide ( $W_{inlet} \sim 10 -$   
 451  $20$  km). In other cases with barrier drowning, widths of inlets overall take lower values  
 452 ( $W_{inlet} \sim 1 - 5$  km). Still, the total fraction below MSL is larger than that at equilib-  
 453 rium, because the number of inlets is very large ( $\sim 15 - 20$ ). Situations in which there  
 454 is barrier drowning with a large number of relatively narrow inlets are characterized by  
 455 high waves ( $H_s \geq 2$  m) and rates of RSLR generally lower than 15 mm/yr. In these  
 456 situations, there is an important deposition of sediment by the littoral drift, which cre-  
 457 ates narrower inlets. In contrast, drowning situations with few and wide inlets only take  
 458 place for  $\dot{\xi} > 15$  mm/yr and intermediate  $H_s$ . In these cases, the combined effect of the  
 459 deepening of the toe of the shoreface (see SI1, Equation 1) and RSLR causes a widen-  
 460 ing of the inlets which can not be balanced by the sediment import of waves. Thus, sim-  
 461 ulations with similar  $\Delta F$  and  $W_b$  may have a significantly different number of inlets.

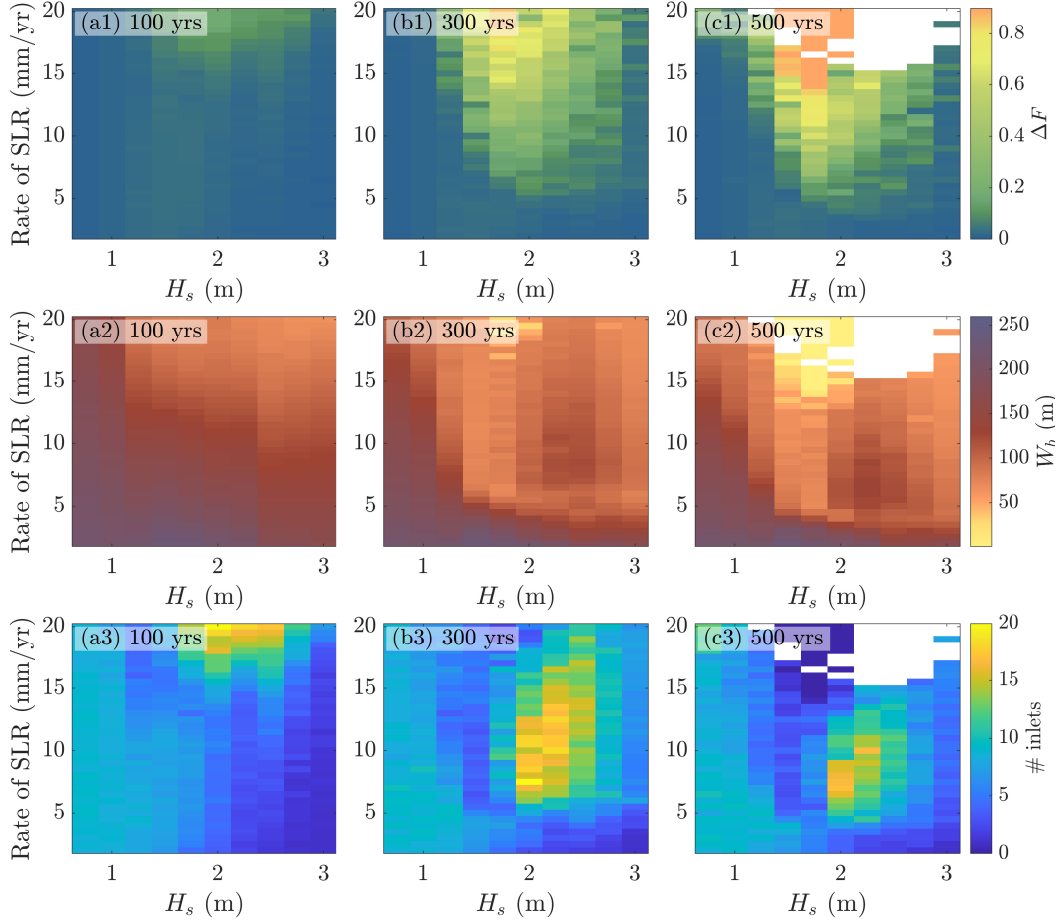


**Figure 8.** For different values of significant wave height  $H_s$  and rate of RSLR  $\dot{\xi}$ : color plots of  $\Delta F$  (**a1,b1,c1**), alongshore mean of barrier width  $W_b$  (**a2,b2,c2**), and number of inlets (**a3,b3,c3**). All three quantities are shown at years 100, 300 and 500 after model spin-up (first, second, and third columns, respectively) and averaged over five simulations. Situations depicted in white in panels (c1,c2,c3) correspond to simulations that became numerically unstable while inlets were widening due to barrier drowning and thus stopped before reaching the year 500. Other simulations yielded a fully drowned barrier, represented by  $\Delta F = 0.9$ ,  $W_b = 0$  and no inlets (top central part of panels c1,c2,c3).

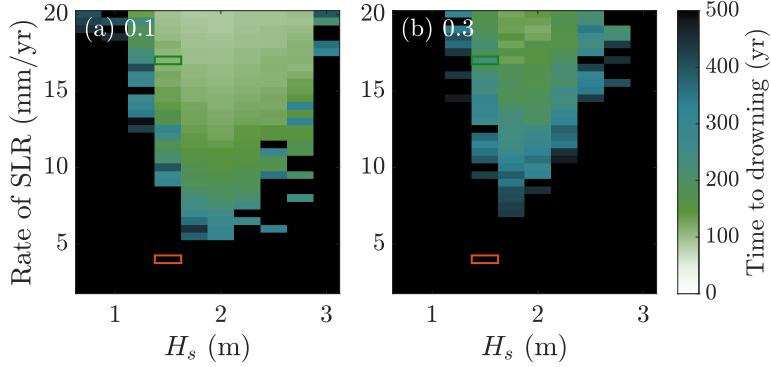


**Figure 9.** Color plots of drowning timescales (time after spin-up needed to reach (a)  $\Delta F = 0.1$  or to reach (b)  $\Delta F = 0.3$ ) for different significant wave heights  $H_s$  and rate of RSLR  $\dot{\xi}$ . Green and red rectangles refer to the situations shown in Figure 6.

462 Depending on the rate of RSLR and on the wave height, the barrier starts drown-  
 463 ing (if it does) after a certain time. In all cases, this is not achieved instantly after the  
 464 rate of RSLR changes, but there is a time lag for the barrier system to adapt. Situations  
 465 in which  $\Delta F$  attains a value of 0.1 or 0.3 are reached earlier for environments with higher  
 466  $\dot{\xi}$  and intermediate  $H_s$  (Figure 9). The time lag depends on  $\dot{\xi}$  because of the gradual evo-  
 467 lution of the inlets cross-sectional area. Still, for the same rate of RSLR, this lag in bar-  
 468 rier response depends on  $H_s$  as well, with intermediate wave heights ( $H_s \sim 2$  m) yield-  
 469 ing the fastest barrier response. Intermediate  $H_s$  causes more drowning due to the deep-  
 470 ening of the shoreface toe, which cannot be counteracted by the increased import of sedi-  
 471 ment into the inlets by the littoral drift. A deepening of the shoreface toe means a larger  
 472 volume of sand that has to adapt to RSLR, thus creating more prone to drowning bar-  
 473 riers. For higher waves, sediment imported by the littoral drift is able to counteract the  
 474 effects of the deepening of the shoreface toe, and it takes longer for a barrier to drown.  
 475 For lower waves, even if the sediment imported by the littoral drift is not so abundant,  
 476 the toe of the shoreface is shallower, thus the whole barrier system adapts faster to RSLR-  
 477 induced drowning. Interestingly, even if most situations deviate from equilibrium, not  
 478 all of them reach a state that is characterized by  $\Delta F = 0.1$  within 500 yrs.

479 Most model simulations of barrier drowning are numerically robust for both BRIE  
 480 and BRIE-D. All quantities shown in Figures 7, 8, 9 have a low standard error compared  
 481 to their mean. For  $\Delta F$ , this value takes generally values below 0.05 and only reaches 0.15  
 482 in situations where  $\Delta F$  is of the order of 0.9. The standard deviation of the mean bar-  
 483 rier width is always below 15 m, and generally around 5 m. Lastly, the standard devia-  
 484 tion of the mean number of inlets is always below 3. Only after 500 yrs of evolution and  
 485 high rates of RSLR ( $\dot{\xi} > 15$  mm/yr) and wave heights ( $H_s > 2$  m) some of the simu-  
 486 lations become numerically unstable during barrier drowning (white patches in Figure 8).  
 487 We further explored the sensitivity of model output to halving the grid size and halv-  
 488 ing the time step and found that differences in  $F$  and  $\Delta F$  were smaller than 3% for the  
 489 situation with default parameter values.

## 490 4 Discussion

### 491 4.1 Choice of Parameters

492 The main objective of this study was to gain insight on the different dynamics re-  
 493 lated to barrier drowning. For simplicity, we have kept wave height, tidal amplitude and

494 storm return period constant through the simulations, albeit they are expected to change  
 495 as  $\dot{\xi}$  increases (Bricheno & Wolf, 2018; Pickering et al., 2012). The chosen values are rep-  
 496 resentative of different barrier systems in the world (Mulhern et al., 2017).

497 Our RSLR scenarios may not be representative of all barrier systems. We have cho-  
 498 sen a spin-up period with  $\dot{\xi} = 2$  mm/yr, followed by 500 yrs with a constant  $\dot{\xi}$  between  
 499 2 and 20 mm/yr through all simulations, which allows for a broader range of scenarios.  
 500 A constant  $\dot{\xi}$  causes an abrupt change in the system after model spin-up, inducing an  
 501 adaptation period of  $\sim 100$  yrs (see Figures 5, 6). The irregularities in the backbarrier  
 502 shoreline just after spin-up (see Figure 4a) may be another manifestation of the abrupt  
 503 change in  $\dot{\xi}$ . Still, these irregularities are smoothed with time and end up disappearing,  
 504 hence we do not consider them to be a sign of model instability.

505 Additional simulations with accelerating rates of RSLR (based on RCP scenarios)  
 506 showed the same tendency as the respective simulations with equivalent constant rates  
 507 of RSLR (see Figure S8). Future studies could, however, study in further detail the ef-  
 508 fects of a gradual increase in rate of RSLR by varying the increase in sea level as well  
 509 as the timescale involved in this gradual evolution. Furthermore, variations in storm re-  
 510 turn period did not cause substantial differences on the results (see Appendix B).

## 511 4.2 Comparison with Earlier Models

512 The cross-shore dynamics reproduced by gradually evolving inlets (BRIE-D model)  
 513 are similar to those obtained with the BRIE model of Nienhuis and Lorenzo-Trueba (2019)  
 514 and with an earlier 2D horizontal barrier island model (which did not include inlets) of  
 515 Lorenzo-Trueba and Ashton (2014). Barrier width eventually attains a constant value  
 516 that depends on  $\dot{\xi}$ . Lorenzo-Trueba and Ashton (2014) found the same behavior and termed  
 517 this state as dynamic equilibrium, because the barrier is still migrating landward, but  
 518 its width does not change. Similarly, the more severe barrier drowning found for larger  
 519 wave heights due to a deepening of the toe of the shoreface is in agreement with results  
 520 of Lorenzo-Trueba and Ashton (2014). Differences include the barrier susceptibility to  
 521 RSLR, which can be lower in BRIE and BRIE-D, because these also account for addi-  
 522 tional landward sediment transports due to inlet and alongshore dynamics.

523 Compared to BRIE, the BRIE-D model computes very high inlet migration rates  
 524 for higher  $\dot{\xi}$  ( $\sim 5$  km/yr, see Figure 5c). These rates mostly appear for narrow barri-  
 525 ers under high rates of RSLR. BRIE-D inlet migration rates exceed rates commonly found  
 526 along modern barrier islands, as indicated by a compilation of Nienhuis and Ashton (2016),  
 527 who found a maximum of 700 m/yr. The BRIE model yields more realistic migration  
 528 rates (of the order of 10 m/yr, see Figure 5d). These differences are caused by different  
 529 migration speeds of the updrift and downdrift tips of the barrier, which allow for inlet  
 530 widening. They may also result in unrealistically large inlet migration rates. Inlet dy-  
 531 namics in BRIE-D are based on Delft3D simulations from Nienhuis and Ashton (2016),  
 532 who computed the distribution of sediment transport between the updrift and downdrift  
 533 tips of the barrier. However, their experiments were performed with barrier widths be-  
 534 tween 250 m and 800 m and inlets narrower than 1 km. Thus, situations with RSLR-  
 535 driven drowning were not included. Future studies should investigate how to better pa-  
 536 rameterize inlet sediment distributions under drowning situations in which the barrier  
 537 becomes narrower, possibly inducing new inlet dynamics. Inlet expansion rather than  
 538 inlet migration is a key mechanism for barrier drowning. Yet, lower inlet migration rates  
 539 would result in a more realistic overall barrier behavior. There would be less frequent  
 540 inlet merging, which would leave less space available for barrier breaching, and would  
 541 result in narrower inlets. Given that changes in inlet cross-sectional area of wider inlets  
 542 only affect inlet width (not depth), having narrower inlets would result in lower  $F$ , and  
 543 probably lower  $\Delta F$ . Given that barrier width shows the same dependencies on wave height

544 and rate of RSLR as  $\Delta F$ , we expect the broad picture to be the same even with more  
 545 realistic inlet migration rates.

546 The observed lag in barrier drowning ( $\Delta F$ ) to the abrupt change in rate of RSLR  
 547 at  $t = 0$  is of the order of  $\sim 100 - 300$  yrs for  $\dot{\xi} = 5 - 20$  mm/yr. Mariotti and Hein  
 548 (2022) found barrier retreat lags changes in  $\dot{\xi}$  by 500 yrs for  $\dot{\xi} = 1 - 10$  mm/yr. They  
 549 explained this lag by the presence of a barrier ‘geomorphic capital’; i.e., the rate of land-  
 550 ward retreat increases only after the sediment reservoir of the barrier has decreased enough,  
 551 and the barrier has adjusted to the new  $\dot{\xi}$ . The BRIE-D model results represent this mech-  
 552 anism as well. The barrier width, as an indicator for its sediment reservoir, decreases first.  
 553 Drowning starts when the barrier width has decreased and the littoral sediment trans-  
 554 port into the inlets can no longer keep up with RSLR. Thus, the barrier first loses part  
 555 of its sediment reservoir, and then starts drowning (increases in  $\Delta F$  after several hun-  
 556 dreds of years, Figure 9).

### 557 4.3 Comparison with Observations

558 The scant observations that exist on barrier drowning are comparable to our sim-  
 559 ulations. The Isles Dernières have experienced gradual drowning during the last  $\sim 200$  yrs  
 560 under a rate of RSLR of 13 mm/yr (Dingler et al., 1993). For this barrier island chain,  
 561  $F$  increased from 0.05 to 0.37 to 0.55, in the years 1853, 1934, and 2015, respectively (obtained  
 562 from aerial images provided in Davis Jr. & FitzGerald, 2010). Simulations performed  
 563 with the BRIE-D model with a rate of RSLR of 13 mm/yr resulted in a similar behav-  
 564 ior. Starting from  $F = 0.06$  after 100 yrs after model spin-up (such that the model has  
 565 adapted to the new  $\dot{\xi}$ ),  $F$  increases up to 0.3 after 80 years of evolution, and to 0.45 af-  
 566 ter another 80 years (see Figure 10). But, situations might not be perfectly compar-  
 567 able. Part of the Isles Dernières barrier drowning could have been the result of marsh loss  
 568 (FitzGerald et al., 2008; Lorenzo-Trueba & Mariotti, 2017) instead of sedimentary deficits.  
 569 BRIE-D does not simulate marsh loss and its influence on the tidal prism, so more re-  
 570 search, and perhaps model updates, are needed to further investigate the causes of Isles  
 571 Dernières barrier drowning. In addition, model outcomes are also sensitive to other fac-  
 572 tors (e.g., shoreface response rate, maximum overwash transports) that are difficult to  
 573 retrieve from field observations. Nevertheless, the gradual disintegration of a barrier sub-  
 574 ject to RSLR and timescales involved are qualitatively similar.

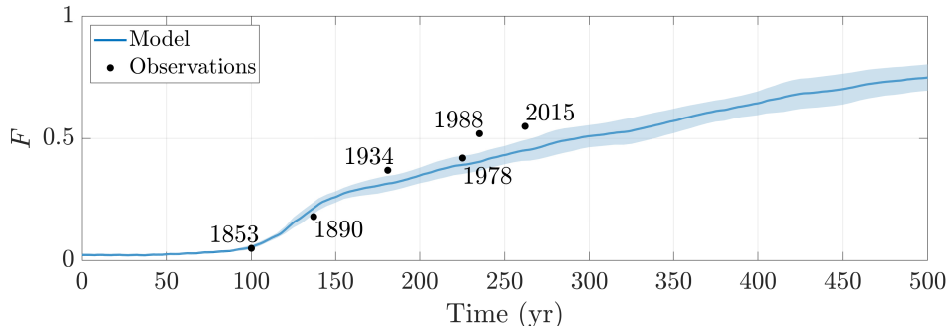


**Figure 10.** Time series of  $F$  for  $\dot{\xi} = 13$  mm/yr, and observations of  $F$  for the Isles Dernières (obtained from aerial images provided in Davis Jr. & FitzGerald, 2010). We align the year 1853 with the model year 100 after spin-up to account for the time needed for the modeled barrier to adapt to the new  $\dot{\xi}$ .

575 Another way to compare our BRIE-D model simulations to observations is to con-  
 576 sider  $F$ , the fraction below MSL. For example, the Wadden Islands have an  $F$  of 0.22,

577 and the New Jersey coast has an  $F$  of 0.03 (Figure 1). The time evolution of  $F$  could  
 578 be obtained from satellite images (Figure 1), available since the 1980s, as well as historic  
 579 maps that go back further. Future work could be designed to model the evolution of bar-  
 580 rier casts and calibrate and/or validate based on observed  $F$ , and then separate between  
 581  $\Delta F$  and  $F_{eq}$  to study potentially ongoing, or future drowning.

#### 582 4.4 Limitations in Modeling and Analysis

583 The BRIE-D model is not able to reproduce all the dynamics involved in barrier  
 584 drowning. For example, we have not modeled the curvature of barrier tips occurring in  
 585 wide inlets when bypassing diminishes (Davis Jr. & FitzGerald, 2010). Future research  
 586 should focus on finding appropriate parametrizations for these dynamics and implement-  
 587 ing them in the BRIE-D model such that the drowning state of a barrier is modeled as  
 588 realistically as possible.

589 Note that model includes a “storm” component, during which breaching occurs (by  
 590 imposing a new inlet). It would be interesting to make the model more stochastic, and  
 591 to link the occurrence and effects of storms to the offshore wave conditions that now only  
 592 affect long-shore and cross-shore transport. A possible approach to do this is to assess  
 593 what the correct scaling is to reduce the effects of stochastic wave heights into a single  
 594 parameter (similar to geomorphic flood for river discharge). Ortiz and Ashton (2016) did  
 595 this for cross-shore transport, but we are not aware of similar scaling rules for overwash  
 596 or other critical processes. It would be interesting to investigate this in future studies.

597 Furthermore, the ebb-tidal delta is not explicitly included in the BRIE-D model  
 598 albeit it is a prominent entity in the sand balance of tidal inlets. Nevertheless, its effects  
 599 on inlet migration rate and the size of the flood-tidal delta are implicitly taken into ac-  
 600 count through its effects on waves and currents (Nienhuis & Ashton, 2016). In that sense,  
 601 the BRIE-D model, as well as the BRIE model, offers a different picture on inlet and bar-  
 602 rier dynamics than that in previous studies, such as that of van de Kreeke (2006).

603 The overwash transport is assumed to be independent of wave height, which is a  
 604 simplification of reality. One of the advantages of the BRIE-D model is the low compu-  
 605 tational effort it requires, involving parametrizations of certain processes. Making over-  
 606 wash dependent on wave height is out of the scope of this study, but we would expect  
 607 to have more severe drowning for lower wave heights because less sediment would be trans-  
 608 ported to the top and back of the barrier. We performed a sensitivity analysis on the  
 609 maximum overwash transport, and saw no important dependencies on the obtained re-  
 610 sults (not shown).

611 Another way to assess the model performance would be to perform a global sensi-  
 612 tivity and uncertainty analysis (GSUA) relating non-linear interactions of model pa-  
 613 rameters to model output (e.g., Convertino et al., 2014). Given that we focused on un-  
 614 derstanding barrier drowning, rather than the interactions between model parameters  
 615 and output, this is out of the scope of the present study.

616 We have studied barrier drowning through the alongshore extent of the barrier be-  
 617 low MSL due to tide-wave imbalance,  $\Delta F$ . We chose this definition because it is straight-  
 618 forward to calculate and easy to compare to observations. Yet, barrier response to high  
 619 rates of RSLR also includes a decrease in barrier height and width. The latter effect was  
 620 considered by computing barrier width over time. The decrease in barrier height has not  
 621 been quantified in this study, but given that it eventually yields drowning of portions  
 622 of the barrier, it is mainly implicitly included when computing  $\Delta F$ . Other ways of quan-  
 623 tifying barrier drowning could have been based on the computation of aerial barrier area  
 624 or volume. These are out of the scope of this study.

625 The BRIE-D model is a useful tool to understand the different mechanisms involved  
 626 in barrier island evolution and, particularly, drowning. In that sense, it should be seen  
 627 as an ‘exploratory model’ (Murray, 2003), aiming to understand a poorly understood phe-  
 628 nomenon (drowning), rather than simulate any barrier system specifically. Specifically,  
 629 the multiple parametrizations used in the model make it very computationally efficient,  
 630 allowing for an in-depth study of the effects of multiple parameters on the response of  
 631 barrier systems. More observations are needed to properly evaluate and compare pro-  
 632 jections from BRIE-D, also in comparison with more process-based models, such as that  
 633 of Mariotti and Hein (2022).

## 634 5 Conclusions

635 Here we aimed to (1) understand the effects of RSLR on the barrier island sedi-  
 636 ment balance, inlet expansion, and the related barrier drowning, (2) examine the tem-  
 637 poral evolution of a barrier island while drowning, as well as quantifying drowning timescales,  
 638 and (3) explore its dependence on model parameters. With our new model (BRIE-D),  
 639 we performed simulations with a wide range of values for significant wave height  $H_s$  and  
 640 rate of RSLR  $\xi$ . From model outputs, we studied barrier island drowning by comput-  
 641 ing the fraction of barrier alongshore extent below MSL, that caused by tide-wave im-  
 642 balance, the alongshore mean of the barrier width, and the number of inlets.

643 We found large effects of inlet dynamics on barrier drowning, making it important  
 644 to include these effects to study the future of barrier islands. Effects of RSLR on inlets  
 645 manifest as an increase in inlet width and number. Barriers drown faster in simulations  
 646 that include feedbacks between tidal inlet dynamics and the cross-shore barrier evolu-  
 647 tion. Nevertheless, barrier response to changes in rates of RSLR remains slow at timescales  
 648 of  $\sim 100$ s of years for common barrier characteristics. During this adaptation period,  
 649 first the barrier loses part of its sediment reservoir through a decrease in barrier width.  
 650 After this period, barrier width stabilizes but inlets expand until the barrier drowns. Spe-  
 651 cific timescales for barrier drowning will vary between barrier island chains, and should  
 652 be interpreted to be general rather than specific.

653 We expect environments with intermediate wave heights to be most sensitive to RSLR-  
 654 induced drowning. Lower wave environments have shallower depth of closure and thus  
 655 respond faster to RSLR. Higher waves trigger two opposed mechanisms: a more frequent  
 656 inlet closure, and a more severe barrier drowning. The former is caused by the larger amount  
 657 of sediment imported into the inlet system, whereas the latter is a result of the deeper  
 658 shoreface toe, which makes a barrier system more prone to drowning.

## 659 Appendix A Default Model Parameters

660 Unless stated otherwise model parameters take their default values, given in Ta-  
 661 ble A1.

## 662 Appendix B Sensitivity Analysis

663 We performed a sensitivity analysis for the main parameters that control the sys-  
 664 tem: tidal amplitude  $a_0$ , significant wave height  $H_s$ , wave period  $T_p$ , rate of RSLR  $\xi$ , wave  
 665 asymmetry  $a$ , inlet aspect ratio  $\gamma_{aspect}$ , storm return period  $T_{storm}$ , maximum overwash  
 666 transport  $Q_{ow,max}$  and the suspended sediment transport efficiency factor  $e_s$ , which con-  
 667 trols the shoreface transport. We varied each of the parameters around  $\pm 50\%$  of their  
 668 default values and computed the fraction of the barrier alongshore extent below MSL  
 669 ( $F$ ) at three different stages: at years 100, 300 and 500 after model spin-up. For each  
 670 set of parameters we created five realizations, from which we computed  $F$  and the stan-  
 671 dard error of the mean. We found clear patterns and deviations from the default case

**Table A1.** Default values of model parameters. Shortened references are as follows: LTA14 (Lorenzo-Trueba & Ashton, 2014), B80 (Bowen, 1980), M17 (Mulhern et al., 2017), AM06 (Ashton & Murray, 2006), SZ09 (de Swart & Zimmerman, 2009), R13 (Roos et al., 2013), N15 (Nienhuis et al., 2015).

Name	Value	Units	Explanation
$\rho_w$	1025	kg m <sup>-3</sup>	Density of water
$\omega$	$1.4 \cdot 10^{-4}$	s <sup>-1</sup>	Offshore tidal radial frequency
$g$	9.81	m s <sup>-2</sup>	Gravitational acceleration
$R$	1.65	–	Submerged specific gravity of sediment
$e_s$	0.01	–	Suspended sediment transport efficiency factor (LTA14)
$c_s$	0.01	–	Friction factor (B80)
$n$	0.05	s m <sup>-1/3</sup>	Manning roughness coefficient
$\dot{\xi}$	10	m yr <sup>-1</sup>	Rate of RSLR
$H_s$	1.5	m	Significant wave height in deepwater (M17)
$a_0$	0.8	m	Offshore tidal amplitude (M17)
$T_{storm}$	10	yr	Minimum period between inlet forming storms
$T_p$	10	s	Peak wave period
$a$	0.8	–	Wave asymmetry (AM06)
$h$	0.2	–	Wave highness (AM06)
$\gamma_{aspect}$	0.005	–	Inlet aspect ratio ( $\gamma_{aspect} = D_{inlet}/W_{inlet}$ )
$u_e$	1	m/s	Tidal inlet equilibrium velocity (SZ09)
$H_{crit}$	2	m	Critical barrier height (LTA14)
$W_{b,crit}$	200	m	Critical barrier width (LTA14)
$Q_{ow,max}$	50	m <sup>3</sup> m <sup>-1</sup> yr <sup>-1</sup>	Maximum overwash transport (LTA14)
$L_{min}$	5	km	Minimum distance between tidal inlets (R13)
$L_b$	50	km	Length of barrier chain
$s_{background}$	$10^{-3}$	–	Background slope (LTA14)
$k$	0.06	m <sup>3/5</sup> s <sup>-6/5</sup>	Alongshore sediment transport constant (N15)
$\Delta y$	100	m	Alongshore grid spacing
$\Delta t$	0.05	yr	Time step

672 for only four of the eight parameters:  $a_0$ ,  $H_s$ ,  $\dot{\xi}$  and  $\gamma_{aspect}$ . We also add the results for  
673  $T_{storm}$  given its relevance in inlet formation (see Figure B1). Among these five, largest  
674 variations were observed for the significant wave height  $H_s$  and the rate of RSLR  $\dot{\xi}$ . Thus,  
675 we decided to study the dependence of the model on these parameters in more detail (see  
676 Section 3.3).

677 Increasing the tidal amplitude, results in a generally larger  $F$  due to a gain in tidal  
678 prism, which increases the amount of sediment exported by tidal currents (de Swart &  
679 Zimmerman, 2009). Lower tidal amplitudes cause a lower  $F$  due to less sediment being  
680 exported by tidal currents.

681 Regarding the significant wave height, we observe two opposite responses. Depend-  
682 ing on the time after model spin-up, higher waves may produce a decrease or an increase  
683 in  $F$ . This is explained by distinguishing two processes caused by high waves: (1) higher  
684 waves tend to import more sediment into an inlet, thereby favoring its closure (Escoffier,  
685 1940), and (2) higher waves affect the sediment at deeper bed levels, causing a larger depth  
686 of closure (Houston, 1995). A larger depth of closure means that a larger volume of sand  
687 responds to sea level variations, yielding a system that is more prone to drowning. Af-  
688 ter 100 yrs, an increase in significant wave height decreases  $F$  to  $-0.03$ , while a decrease  
689 in  $H_s$  increases  $F$  up to  $+0.02$ . This is because at this stage the first mechanism dom-  
690 inates. Nevertheless, after 300 or 500 yrs of model evolution, when the effects of RSLR-  
691 induced drowning are more prevalent, a decrease in  $H_s$  causes a decrease in  $F$ . There

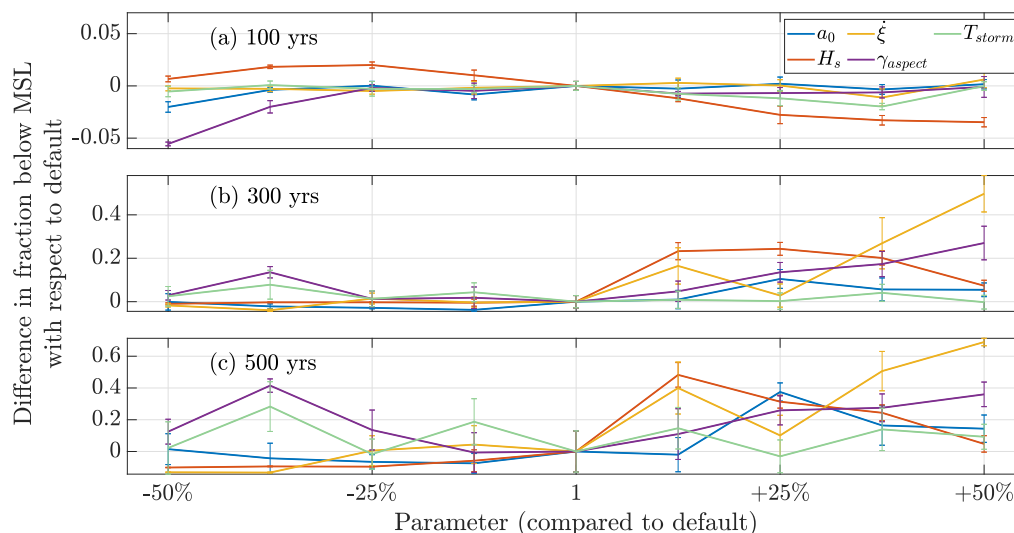


**Figure B1.** Differences in fraction below MSL with respect to the default case when varying different morphodynamic parameters at **(a)** 100 yrs, **(b)** 300 yrs and **(c)** 500 yrs after model spin up. Note the different scales in the vertical axis.

692 is a clear peak in  $F$  for intermediate wave heights. In these situations the second process  
 693 dominates the evolution of the barrier system, inducing more severe drowning.

694 Increasing the rate of RSLR results in more severe drowning, inducing an increase  
 695 in  $F$  of up to  $+0.68$  by the year 500 for the most extreme case. Note that effects of drown-  
 696 ing are only visible from year 300 onwards. In contrast, decreasing the rate of RSLR de-  
 697 creases  $F$  by  $-0.13$  because there is less drowning.

698 An increase in inlet aspect ratio creates narrower inlets for the same cross-sectional  
 699 area, thereby yielding a slightly lower  $F$  at year 100 ( $-0.01$ ). However, in the years 300  
 700 and 500 an increase in inlet aspect ratio results in the opposite effect, yielding an increase  
 701 in  $F$  of up to  $+0.36$ . Lowering the inlet aspect ratio makes shallower inlets, increasing  
 702 the bottom friction. This causes the inlets to be more susceptible to closing, decreasing  
 703 thus  $F$  at year 100 by  $-0.05$ . However, at 300 or 500 yrs after model spin-up,  $F$  increases  
 704 for lower values of the inlet aspect ratio. These differences in behavior between earlier  
 705 and latter times suggest that the dependence of the barrier evolution on the inlet aspect  
 706 ratio is susceptible to RSLR-driven drowning, similarly to the situation obtained when  
 707 varying  $H_s$ .

708 The model shows a weak dependency on the storm return period. A decrease in  
 709 storm return period causes more frequent breaching, yielding a larger  $F$ . Larger  $T_{storm}$   
 710 shows no important differences in  $F$  during the first 300 yrs of evolution. At the year  
 711 500, a larger  $T_{storm}$  seems to suggest a larger  $F$ . This asymmetry in behavior means that  
 712 at this stage the evolution of the barrier system is controlled by RSLR-driven drown-  
 713 ing.

## 714 Open Research

715 The code for the BRIE-D model is accessible from [https://doi.org/10.5281/](https://doi.org/10.5281/zenodo.7353693)  
 716 [zenodo.7353693](https://doi.org/10.5281/zenodo.7353693) (Portos-Amill et al., 2022).

717 **Acknowledgments**

718 We thank Kristen Splinter, Laura J. Moore and two anonymous reviewers for help-  
719 ful feedback that improved this manuscript.

720 **References**

- 721 Ashton, A. D., & Lorenzo-Trueba, J. (2018). Morphodynamics of barrier response  
722 to sea-level rise. In L. J. Moore & A. B. Murray (Eds.), *Barrier Dynamics and*  
723 *Response to Changing Climate* (pp. 277–304). Cham: Springer International  
724 Publishing. doi: 10.1007/978-3-319-68086-6\_9
- 725 Ashton, A. D., & Murray, A. B. (2006). High-angle wave instability and emergent  
726 shoreline shapes: 1. Modeling of sand waves, flying spits, and capes. *Journal of*  
727 *Geophysical Research: Earth Surface*, 111(F4). doi: 10.1029/2005JF000422
- 728 Beets, D. J., & van der Spek, A. J. F. (2000). The Holocene evolution of the bar-  
729 rier and the back-barrier basins of Belgium and the Netherlands as a function  
730 of late Weichselian morphology, relative sea-level rise and sediment supply.  
731 *Netherlands Journal of Geosciences - Geologie en Mijnbouw*, 79(1), 3–16. doi:  
732 10.1017/S0016774600021533
- 733 Bowen, A. (1980). Simple models of nearshore sedimentation: Beach profiles and  
734 longshore bars. In S. B. McCann (Ed.), *The Coastline of Canada* (Vol. 80-10,  
735 p. 1-11). Geological Survey of Canada.
- 736 Bricheno, L. M., & Wolf, J. (2018). Future wave conditions of Europe, in response to  
737 high-end climate change scenarios. *Journal of Geophysical Research: Oceans*,  
738 123(12), 8762-8791. doi: 10.1029/2018JC013866
- 739 Convertino, M., Muñoz-Carpena, R., Chu-Agor, M. L., Kiker, G. A., & Linkov, I.  
740 (2014). Untangling drivers of species distributions: Global sensitivity and  
741 uncertainty analyses of MaxEnt. *Environmental Modelling & Software*, 51,  
742 296-309. doi: 10.1016/j.envsoft.2013.10.001
- 743 Davis Jr., R. A., & FitzGerald, D. M. (2010). Barrier systems. In *Beaches and*  
744 *Coasts*. Wiley.
- 745 Deaton, C. D., Hein, C. J., & Kirwan, M. L. (2017). Barrier island migration dom-  
746 inates ecogeomorphic feedbacks and drives salt marsh loss along the Virginia  
747 Atlantic Coast, USA. *Geology*, 45(2), 123-126. doi: 10.1130/G38459.1
- 748 de Swart, H., & Zimmerman, J. (2009). Morphodynamics of tidal inlet systems.  
749 *Annual Review of Fluid Mechanics*, 41(1), 203-229. doi: 10.1146/annurev.fluid  
750 .010908.165159
- 751 Dingler, J. R., Reiss, T. E., & Plant, N. G. (1993). Erosional patterns of the Isles  
752 Dernières, Louisiana, in relation to meteorological influences. *Journal of*  
753 *Coastal Research*, 112–125.
- 754 Escoffier, F. (1940). The stability of tidal inlets. *Shore and Beach*(8), 114-115.
- 755 FitzGerald, D. M., Fenster, M. S., Argow, B. A., & Buynevich, I. V. (2008). Coastal  
756 impacts due to sea-level rise. *Annual Review of Earth and Planetary Sciences*,  
757 36(1), 601-647. doi: 10.1146/annurev.earth.35.031306.140139
- 758 Houston, J. (1995). Beach-fill volume required to produce specified dry beach width.  
759 In *Coastal Engineering Technical Note* (p. 11-32). US Army Engineer Water-  
760 ways Experiment Station Vicksburg, Mississippi.
- 761 Hume, T. M., & Herdendorf, C. E. (1992). Factors controlling tidal inlet characteris-  
762 tics on low drift coasts. *Journal of Coastal Research*, 8(2), 355–375.
- 763 Leatherman, S. P. (1983). Barrier dynamics and landward migration with Holocene  
764 sea-level rise. *Nature*, 301(5899), 415–417.
- 765 Lorenzo-Trueba, J., & Ashton, A. D. (2014). Rollover, drowning, and discontinuous  
766 retreat: Distinct modes of barrier response to sea-level rise arising from a sim-  
767 ple morphodynamic model. *Journal of Geophysical Research: Earth Surface*,  
768 119(4), 779-801. doi: 10.1002/2013JF002941

- 769 Lorenzo-Trueba, J., & Mariotti, G. (2017). Chasing boundaries and cascade effects  
770 in a coupled barrier-marsh-lagoon system. *Geomorphology*, *290*, 153-163. doi:  
771 10.1016/j.geomorph.2017.04.019
- 772 Mariotti, G., & Hein, C. J. (2022). Lag in response of coastal barrier-island retreat  
773 to sea-level rise. *Nature Geoscience*, *15*(8), 633–638. doi: 10.1038/s41561-022  
774 -00980-9
- 775 Mellett, C. L., & Plater, A. J. (2018). Drowned barriers as archives of coastal-  
776 response to sea-level rise. In L. J. Moore & A. B. Murray (Eds.), *Barrier Dy-*  
777 *namics and Response to Changing Climate* (pp. 57–89). Cham: Springer Inter-  
778 national Publishing. doi: 10.1007/978-3-319-68086-6\_2
- 779 Moore, L. J., List, J. H., Williams, S. J., & Stolper, D. (2010). Complexities in  
780 barrier island response to sea level rise: Insights from numerical model exper-  
781 iments, North Carolina Outer Banks. *Journal of Geophysical Research: Earth*  
782 *Surface*, *115*(F3). doi: 10.1029/2009JF001299
- 783 Mulhern, J. S., Johnson, C. L., & Martin, J. M. (2017). Is barrier island morphol-  
784 ogy a function of tidal and wave regime? *Marine Geology*, *387*, 74-84. doi: 10  
785 .1016/j.margeo.2017.02.016
- 786 Murray, A. B. (2003). Contrasting the goals, strategies, and predictions associ-  
787 ated with simplified numerical models and detailed simulations. *Geophysical*  
788 *Monograph-American Geophysical Union*, *135*, 151–168.
- 789 Nienhuis, J. H., & Ashton, A. D. (2016). Mechanics and rates of tidal inlet mi-  
790 gration: Modeling and application to natural examples. *Journal of Geophysical*  
791 *Research: Earth Surface*, *121*(11), 2118-2139. doi: 10.1002/2016JF004035
- 792 Nienhuis, J. H., Ashton, A. D., & Giosan, L. (2015). What makes a delta wave-  
793 dominated? *Geology*, *43*(6), 511-514. doi: 10.1130/G36518.1
- 794 Nienhuis, J. H., & Lorenzo-Trueba, J. (2019). Simulating barrier island re-  
795 sponse to sea level rise with the barrier island and inlet environment (BRIE)  
796 model v1.0. *Geoscientific Model Development*, *12*(9), 4013–4030. doi:  
797 10.5194/gmd-12-4013-2019
- 798 Ortiz, A. C., & Ashton, A. D. (2016). Exploring shoreface dynamics and a mecha-  
799 nistic explanation for a morphodynamic depth of closure. *Journal of Geophysi-*  
800 *cal Research: Earth Surface*, *121*(2), 442-464. doi: 10.1002/2015JF003699
- 801 Palmer, M. D., Gregory, J. M., Bagge, M., Calvert, D., Hagedoorn, J. M., Howard,  
802 T., . . . Spada, G. (2020). Exploring the drivers of global and local sea-  
803 level change over the 21st century and beyond. *Earth’s Future*, *8*(9). doi:  
804 10.1029/2019EF001413
- 805 Pickering, M., Wells, N., Horsburgh, K., & Green, J. (2012). The impact of future  
806 sea-level rise on the European Shelf tides. *Continental Shelf Research*, *35*, 1-  
807 15. doi: 10.1016/j.csr.2011.11.011
- 808 Portos-Amill, L., Nienhuis, J. H., & de Swart, H. (2022). *LPortos-Amill/BRIE-D:*  
809 *BRIE-D model*. [Software]. Zenodo. (v1.0) doi: 10.5281/zenodo.7353693
- 810 Reef, K. R. G., Roos, P. C., Andringa, T. E., Dastgheib, A., & Hulscher, S. J. M. H.  
811 (2020). The impact of storm-induced breaches on barrier coast systems subject  
812 to climate change—A stochastic modelling study. *Journal of Marine Science*  
813 *and Engineering*, *8*(4), 271. doi: 10.3390/jmse8040271
- 814 Roos, P. C., Schuttelaars, H. M., & Brouwer, R. L. (2013). Observations of barrier  
815 island length explained using an exploratory morphodynamic model. *Geophysi-*  
816 *cal Research Letters*, *40*(16), 4338–4343. doi: 10.1002/grl.50843
- 817 Sanders, J. E., & Kumar, N. (1975). Evidence of shoreface retreat and in-place  
818 “drowning” during Holocene submergence of barriers, shelf off Fire Island, New  
819 York. *Geological Society of America Bulletin*, *86*(1), 65–76.
- 820 Stolper, D., List, J. H., & Thieler, E. R. (2005). Simulating the evolution of  
821 coastal morphology and stratigraphy with a new morphological-behaviour  
822 model (GEOMBEST). *Marine Geology*, *218*(1), 17-36. doi: 10.1016/  
823 j.margeo.2005.02.019

- 824 van de Kreeke, J. (2004). Equilibrium and cross-sectional stability of tidal inlets:  
825 application to the Frisian Inlet before and after basin reduction. *Coastal Engi-*  
826 *neering*, 51(5), 337-350. doi: 10.1016/j.coastaleng.2004.05.002
- 827 van de Kreeke, J. (2006). An aggregate model for the adaptation of the morphol-  
828 ogy and sand bypassing after basin reduction of the Frisian Inlet. *Coastal En-*  
829 *gineering*, 53(2), 255-263. doi: j.coastaleng.2005.10.013